Environmental Microbiology
April 2019, Volume 21 Issue 4 Pages 1452-1465
https://doi.org/10.1111/1462-2920.14579
https://archimer.ifremer.fr/doc/00486/59759/

Diatoms shape the biogeography of heterotrophic prokaryotes in early spring in the Southern Ocean

Liu Yan [1], Debeljak Pavla [1, 2], Rembauville Mathieu [1], Blain Stéphane [1], Obernosterer Ingrid [1, *]

[1] Sorbonne Université, CNRSLaboratoire d'Océanographie Microbienne (LOMIC), 66650 Banyuls-sur-Mer ,France
[2] Department of Limnology and Bio-OceanographyUniversity of Vienna, 1090 Vienna, Austria

* Corresponding author : Ingrid Obernosterer, email address : ingrid.obernosterer@obs-banyuls.fr

Abstract :

The interplay among microorganisms profoundly impacts biogeochemical cycles in the ocean. Culture-based work has illustrated the diversity of diatom–prokaryote interactions, but the question of whether these associations can affect the spatial distribution of microbial communities is open. Here, we investigated the relationship between assemblages of diatoms and of heterotrophic prokaryotes in surface waters of the Indian sector of the Southern Ocean in early spring. The community composition of diatoms and that of total and active prokaryotes were different among the major ocean zones investigated. We found significant relationships between compositional changes of diatoms and of prokaryotes. In contrast, spatial changes in the prokaryotic community composition were not related to geographic distance and to environmental parameters when the effect of diatoms was accounted for. Diatoms explained 30% of the variance in both the total and the active prokaryotic community composition in early spring in the Southern Ocean. Using co-occurrence analyses, we identified a large number of highly significant correlations between abundant diatom species and prokaryotic taxa. Our results show that key diatom species of the Southern Ocean are each associated with a distinct prokaryotic community, suggesting that diatom assemblages contribute to shaping the habitat type for heterotrophic prokaryotes.

Introduction

Marine autotrophic and heterotrophic microbes are tightly coupled on spatial and temporal scales. The production and remineralization of dissolved organic matter (DOM) is a basic interaction that mediates the fluxes of large quantities of carbon and energy between these components of the microbial community (Ducklow, 2006). Roughly half of recent primary production is taken up by heterotrophic microbes, resulting in a respiration that is several-fold higher than the annual increase in atmospheric carbon dioxide (CO_2) of 4 Gt (Ciais *et al*., 2014). Diatoms are ubiquitous phototrophic microbes known to produce large quantities of DOM (Biddanda and Benner, 1997; Myklestad, 2000). This group is abundant at high latitudes and dominates phytoplankton blooms in the nutrient-rich, cold surface waters of the Southern Ocean (Smetacek *et al*., 2004; Quéguiner, 2013; Assmy *et al*., 2013; Malviya *et al*., 2016), thereby influencing the dynamics of heterotrophic microbes.

Phytoplankton blooms markedly affect the prokaryotic community composition (see reviews by Buchan *et al*., 2014; Bunse and Pinhassi, 2017). The successional shifts were linked to the temporal modifications in the quantity and quality of the phytoplankton-derived DOM providing new niches for either opportunistic prokaryotic taxa or those adapted in the preferential utilization of the compounds released (Rinta-Kanto *et al*., 2012; Sarmento and Gasol *et al*., 2012; Teeling *et al*., 2012; Li *et al*., 2018). Using the exudate of a common diatom species as growth substrate in an experimental approach and *in situ* observations allowed to establish a link between substrate preferences of several prokaryotic taxa and their presence during spring phytoplankton blooms in the Southern Ocean (Landa *et al*., 2016). The reported co-occurrence patterns between eukaryotic and prokaryotic taxa extend the potential importance of biotic interactions to larger temporal and spatial scales (Gilbert *et al*., 2012; Lima-Mendez *et al*., 2015; Milici *et al*., 2016; Needham and Fuhrman, 2016; Zhou *et al*.,

2018). These networks could in part be driven by the exchange of a suite of metabolites, discovered in experimental studies using model organisms.

The interplay between autotrophic and heterotrophic microbes could be governed by mechanisms that are species-specific (Amin *et al*., 2012). The production of compounds of the vitamin B group, such as B1 by *Marinomonas* sp. SBI22 (Paerl *et al*., 2017), B2 (Johnson *et al*., 2016) and B12 by *Ruegeria pomeroyi* DSS-3 (Durham *et al*., 2015) was shown to support the growth of the phototrophs *Ostreococcus lucimarinus* and *Thalassiosira pseudonana*, respectively. The exchange of nitrogen and carbon governs certain associations between the nitrogen fixing cyanobacterium UCYN-A and the unicellular algae *Braarudosphaera bigelowii* (Thompson *et al*., 2012; Zehr *et al*., 2015). The production of siderophores by *Marinobacter* sp. DG879 that help acquire iron could promote interactions with phytoplankton, such as the dinoflagellate *Scrippsiella trochoidea* (Amin *et al*., 2009). Diatom cell division was recently shown to be regulated by the excretion of hormones released by prokaryotes based on the co-cultured *Pseudo-nitzschia multiseries* with *Sulfitobacter* sp. SA11 and *Thalassiosira pseudonana* with *Croceibacter atlanticus* (Amin *et al*., 2015; van Tol *et al*., 2017). These findings in combination with the observed co-occurrence of microbial taxa (Gilbert *et al*., 2012; Lima-Mendez *et al*., 2015; Milici *et al*., 2016; Needham and Fuhrman, 2016; Zhou *et al*., 2018) raise the question of whether interactions have the potential to drive biogeographic patterns of microbial communities in the aquatic environment.

The objective of the present study was to investigate the association between diatom assemblages and the prokaryotic community composition on a spatial scale. We specifically asked the question of whether diatom community composition can explain biogeographic

patterns of prokaryotes. Both the total and potentially active prokaryotic community was considered with the aim to identify differences in their respective associations with diatoms. We explored this question in surface waters of the Indian sector of the Southern Ocean in early spring, when diatoms are the major contributor to phytoplankton biomass. We concurrently tested for the possible effects of geographic distance and environmental parameters, key factors identified in previous biogeographic studies of prokaryotic communities (see review by Hanson *et al*., 2012).

Results

Environmental context

Our study was conducted over a large spatial distance (≈ 3000 km) in the Indian sector of the Southern Ocean, covering four oceanic zones, the subtrophical zone (STZ), the subantarctic zone (SAZ), the polar front zone (PFZ) and the antarctic zone (AAZ) (Table 1; Fig. 1). Gradients in environmental parameters, determined in seawater collected at 10 m, were particularly pronounced between the STZ and the SAZ, while overall minor variations within surface waters of the PFZ and AAZ were detectable (see Table S1 for dissolved oxygen and salinity). Temperature decreased from 20.09 °C in the STZ to -1.12 °C at the southernmost station SI. Concentrations of DOC dropped from roughly 70 µM in the subtropical zone to 50 µM within and south of the SAZ. An opposite trend was observed for the major inorganic nutrients nitrate and nitrite, phosphate and silicic acid. Abundances of heterotrophic prokaryotes decreased by a factor of 3 from the STZ to the southernmost stations O11 and SI. The coastal site BDT (1 nautical mile from shore, 50 m overall depth) within a bay of Kerguelen Island was characterized by higher DOC concentrations and lower Synechococcus abundances, and much lower diatom abundances as compared to the stations located within the PFZ. Concentrations of chlorophyll *a* had no pronounced N to S gradient

and highest concentrations were detectable above the Kerguelen plateau (stations A3-1 and A3-2), paralleled by the highest diatom abundances. Diatoms dominated in terms of abundance over dinoflagellates at all sampling sites except at station O22 in the STZ. Diatom carbon biomass accounted for 2-14% of total phytoplankton biomass in subtropical waters, while its contribution was on average 59% for all other stations (Rembauville *et al*., 2017).

Diatom community composition

The composition of the diatom community, determined by microscopic observations, was significantly different among the 4 ocean zones (ANOSIM, $R = 0.78$, $P < 0.01$) based on Bray-Curtis dissimilarity. Samples originating from the SAZ (O25), the PFZ (O12 and TNS6) and the AAZ (A3, O11, KER, FS and SI) formed one main cluster, and samples originating from the STZ (O22 and O24) formed an independent branch, including the coastal site BDT (Fig. 2). Within the main group, separate clusters for the samples from the SAZ, the PFZ, station A3, located above the Kerguelen plateau, and the stations south of Kerguelen Island were detectable. Major diatoms in the STZ were small centric spp. (19-67% of total diatom abundance), corresponding to an assemblage of diatoms < 25 µm that could not be determined to the species level, and *Pseudo-nitzschia* spp. (8-59%), while in the SAZ *Chaetoceros radicans* (51%) and *Chaetoceros socialis* (18%) dominated. In the PFZ *Thalassionema nitzschioides* (~32%), small centric spp. (9-38%), *Fragilariopsis kerguelensis* (7-22%) and *Eucampia antarctica* (2-16%) were the main contributors to the diatom community (Fig. 2). These diatoms contributed also substantially to the community at station A3. However, the dominant species at this site was *Chaetoceros curvisetus,* accounting for 53% of total diatom abundance, followed by *Thalassionema nitzschioides* (22-28%). In surface waters south of Kerguelen Island (O11, KER, FS and SI), *Fragilariopsis kerguelensis* contributed between 15 and 37% of total diatom abundance. *Pseudo-nitzschia* spp. (2-31%),

small centric spp. (3-21%), *Chaetoceros curvisetus* (3-18%), and *Thalassionema nitzschioides* (2-10%) accounted for overall lower and more variable fractions of diatom abundance at these sites.

Composition of total and active prokaryotic **communities**

From the 12 stations, each sampled in biological triplicates, we obtained 36 subsamples for the total (DNA) and 36 subsamples for the active (RNA) prokaryotic community. From the total of 72 subsamples, we obtained 1326 operational taxonomic units (OTUs) defined at 97% similarity based on the 16S rRNA gene amplicon sequencing targeted on the V4 - V5 region. A large number of OTUs (1217) were shared among the DNA and RNA data sets, with 1320 and 1323 OTUs obtained from the DNA and RNA samples, respectively. Unshared OTUs were not abundant in either the DNA or the RNA data set. nMDS ordination analysis showed that prokaryotic communities were significantly different among ocean zones (ANOSIM, R = 0.69, $P < 0.01$) (Fig. 3). The three biological replicates analysed from each station closely clustered together, illustrating the high replicability among samples for both DNA and RNA (Fig. S1). For the subsequent illustrations and analyses, the biological triplicates were pooled separately for the DNA and RNA data sets and the mean relative abundance was calculated for each OTU.

According to OTU abundances, sample assemblages were dominated by Alphaproteobacteria (DNA 42% of the sequences of all samples pooled, RNA 38%), Bacteroidetes (DNA 28%, RNA 34%), Gammaproteobacteria (DNA 18%, RNA 16%) and Cyanobacteria (DNA 9%, RNA 8%), with SAR11, Flavobacteria, Thiomicrospirales and Synechococcales as major sub-taxa respectively (Fig. S2). Deltaproteobacteria and Archaea were not abundant in surface waters (each < 0.6% of sequences pooled from all sites). Dominant OTUs (i.e. ≥ 1% of the sequences in at least one sample) represented similar proportions of the total (DNA) and

active (RNA) communities at a given site (Fig. S2). For clarity, the following brief description is focused on DNA data. Within Alphaproteobacteria, SAR11 was the most abundant taxon, with 2 distinct OTUs belonging to SAR11 Ia being abundant (2-16% of the sequences at a given site) either in the STZ or in the AAZ. Sphingomonadales were present in almost all samples. Within Gammaproteobacteria, one OTU belonging to Thiomicrospirales had high relative abundances in the SAZ, PFZ (except for BDT) and AAZ (3-9%), and groups such as SAR86, Pseudomonadales and Alteromonadales revealed abundances < 2%. Within Flavobacteria, 2 OTUs belonging to the NS2b marine group were abundant in the SAZ, PFZ (except for BDT) and AAZ (3-12%), with highest relative abundances at station SI. Marine group NS9 was present with relatively high abundance at station A3-2 (~ 4%). SAR324 marine group belonging to Deltaproteobacteria represented 1-2% of the reads at the AAZ stations, except for A3-2. Cyanobacteria had high abundances in the STZ and at station BDT, represented by Synechococcus and Prochlorococcus. Archaeal Thaumarchaeota varied between 0.5-1% at stations KER, FS, A3-1 and A3-2.

Linking prokaryotic **and diatom community composition**

To explore the question of whether prokaryotic community composition was linked to the diatom assemblages, we calculated the dissimilarity for each pair of samples of both prokaryotic and diatom communities. Based on the Mantel test, we observed significant relationships between changes in the diatom assemblages and in the total (DNA) (Fig. 4; R = 0.55; $P < 0.01$) and active (RNA) (Fig. S3; R = 0.55; $P < 0.01$) prokaryotic communities for the Southern Ocean samples (SAZ, PFZ and AAZ; excluding BDT). This illustrates that the dissimilarity in the composition of each the total and active prokaryotic community increases with an increasing dissimilarity of the diatom assemblages. Significant relationships were also

obtained for the entire data set, including the two stations in the STZ and station BDT (Fig. S4; $R = 0.78$, $P < 0.01$). We then tested the potential influence of geographic distance and environmental parameters. Geographic distance was not correlated to the changes in prokaryotic community composition (Mantel test, $P > 0.05$), as shown by the lack of any significant distance decay relationship (Fig. S5). To determine the potential influence of environmental parameters, we performed a canonical correspondence analysis. For the Southern Ocean, temperature explained in part the separate clustering of the SAZ sample (Fig. S6; ANOVA, $P < 0.05$). For the entire data set, temperature, salinity and DOC explained the separate clustering of the samples from the STZ (Fig. S6; ANOVA, $P < 0.05$). We then applied the partial Mantel test to consider concurrently the influence of diatoms and geographic distance, and diatoms and environmental parameters on prokaryotic community composition (Table 2). Diatoms explained significantly the variance of the prokaryotic community composition, whereas geographic distance or environmental variables alone could not when the effect of diatoms on prokaryotic communities was controlled for (Table 2; overall $P < 0.05$). In addition, within the AAZ, the relationship between prokaryotic communities and geographic distance was not significant with and without controlling for the effect of diatoms ($P > 0.05$). Diatom community composition explained 30% of the variance in both the total and active Southern Ocean prokaryotic community composition. Including the two stations in the STZ and BDT, the respective variances explained 70% and 50% (Table S2). It was interesting to note that in contrast to prokaryotes, diatom community composition could be explained by the combined environmental parameters and in particular, salinity, dissolved oxygen, nitrate and nitrite (Table S2).

The potential relationships between dominant diatom species and prokaryotic OTUs were further investigated using co-occurrence analysis (Fig. 5). Diatom species and prokaryotic OTUs with ≥ 1% relative abundance in at least one sample were considered. The correlation

patterns were similar for total and active prokaryotic communities. The cluster analysis revealed several groups of diatoms, each associated with distinct prokaryotic assemblages. For the description of these groups we focus on a few representative diatom species. *Fragilariopsis kerguelensis*, *Thalassionema nitzschoides* and *Chaetoceros curvisetus* were numerically abundant at several Southern Ocean sites (Fig. 2), and revealed strong positive correlations ($r \geq 0.6$) with distinct prokaryotic OTUs. *Fragilariopsis kerguelensis* was strongly positively correlated with several Flavobacteria OTUs belonging to groups NS5, NS9 and NS10. Positive correlations were also found with alphaproteobacterial OTUs belonging to the SAR11 I and SAR116 clades, and to Rhodobacterales, further with gammaproteobacterial OTUs belonging to Pseudomonadales, OM182 and SAR86, and to one OTU of the deltaprotebacterial SAR324 group. *Thalassionema nitzschoides* was positively correlated with Flavobacteria OTUs belonging to the NS4, NS7, NS9, *Polaribacter* and *Ulvibacter* groups, several Rhodobacterales OTUs as well as SAR11 Ib. *Chaetoceros curvisetus*, a diatom that accounted for 53% of the diatom abundance at station A3 above the plateau revealed strong correlations with Flavobacteria OTUs exclusively belonging to the NS9 group, one OTU belonging to the gammaproteobacterial Thiomicrospirales, and one OTU belonging to Thaumarchaeota. For comparison, *Chaetoceros radicans* and *Chaetoceros socialis*, dominant diatom species in the SAZ, revealed strong correlations to a distinct set of OTUs belonging to Flavobacteria groups NS2b, NS10 and NS4, to one OTU belonging each to Rhodobacterales, SAR11, SAR86 and Thiomicrospirales. Small centric spp. and *Pseudo-nitzschia* spp., diatoms with overall higher relative abundances in subtropical waters were again associated with distinct OTUs belonging to all major groups. In addition, several strong ($r \geq 0.6$) positive correlations between Cyanobacterial OTUs and diatoms abundant in the STZ and at BDT were detectable.

Discussion

Contemporary environmental selection has widely been identified as one central mechanism for shaping the spatial distribution of heterotrophic microbes in the ocean (reviewed in Hanson *et al*., 2012). Dispersal and drift are additional factors that were identified in biogeographic studies (Lindström and Langenheder, 2012; Wilkins *et al*., 2013). By contrast, the potential influence of the community composition of microorganisms that can interact with heterotrophic microbes has only recently been taken into consideration in this context (Lima-Mendez *et al*., 2015; Milici *et al*., 2016, Zhou *et al*., 2018). The present study reveals that the spatial pattern in the community structure of heterotrophic microbes in surface waters is tightly associated to changes in the diatom assemblages, rather than to geographic distance and environmental conditions. Our survey covers the major oceanographic zones of the Southern Ocean where diatoms are dominant components of the autotrophic community and our results illustrate their potential role in shaping microbial diversity in surface waters of this part of the ocean.

The key diatom species that we identified, based on their high relative abundances at several sites, could be indicative for two broad ecological niches in the Southern Ocean. *Fragilariopsis kerguelensis*, a chain forming, heavily silicified pennate diatom with overall low growth rates is typically associated with high-nutrient-low-chlorophyll (HNLC) systems (Smetacek *et al*., 2004; Quéguiner, 2013). By contrast, small diatoms (<25 µm), such as *Chaetoceros* spp., *Thalassionema nitzschioides* and *Thalassiosira* spp. are more lightly silicified and known to develop rapidly under favourable conditions, such as in response to iron supply by natural fertilization in the region east of Kerguelen Island (Blain *et al*., 2007; Lasbleiz *et al*., 2016) or to mesoscale artificial iron additions (Assmy *et al*., 2013). *Fragilariopsis kerguelensis* was associated to several OTUs of the SAR11 Ia and SAR116

clades and OTUs belonging to OM182 and SAR86, groups that were previously characterized as oligotrophs to be adapted to conditions of low resource supply (Sowell *et al*., 2009; Yooseph *et al*., 2010; Swan *et al*., 2013). Noticeably strong correlations were also found for deltaproteobacterial SAR324 OTUs. Members of this group are chemolithotrophic (Swan *et al*., 2011; Sheik, 2014) and thus likely better adapted to oligotrophic conditions. By contrast, *Thalassionema nitzschoides* and *Chaetoceros curvisetus* had strong correlations with OTUs that were previously identified as rapid responders to phytoplankton blooms, as for example the flavobacterial OTUs *Polaribacter*, *Ulvibacter* and OTUs from the NS7 group (Buchan *et al*., 2014). Among these, *Polaribacter* has frequently been observed in temperate (Teeling *et al*., 2012; Klindworth *et al*., 2014; Needham and Fuhrman, 2016) and polar regions under bloom conditions (Williams *et al*., 2013; Delmont, 2014; Luria *et al*., 2016; Dadaglio *et al*., 2018) and in response to labile organic matter supply (Dinasquet *et al*., 2017; Luria *et al*., 2017; Tada *et al*., 2017). Similarly, *Rhodobacterales* had a higher number of strong positive correlations with *Thalassionema nitzschoides* and *Chaetoceros curvisetus* than with *Fragilariopsis kerguelensis.* The rapid response of the above mentioned OTUs to phytoplankton blooms has been attributed to their uptake capacities of specific phytoplankton-derived substrates, using functional profiling based on metatranscriptomics (Teeling *et al*., 2012; Rinta-Kanto *et al*., 2012; Beier *et al*., 2015) and metaproteomics (Li *et al*., 2018).

We expected the composition of total and active prokaryotes to be different, but the spatial distribution and the co-occurrence patterns revealed to be highly similar between these communities. The use of RNA-based approaches to distinguish the active microbial community members from inactive or dormant ones is based on the relationship between cellular content of ribosomal RNA (rRNA) and metabolic activity (Kerkhof and Ward, 1993; Poulsen *et al*., 1993). Several limitations were pointed out (Blazewicz *et al*., 2013), including

differences in the relationship between rRNA content and growth rate among taxa, and the possibly high rRNA content of dormant and inactive cells (Flärdh *et al*., 1992; Fegatella *et al*., 1998). Previous investigations in the study region have shown that bulk prokaryotic production and growth rates in early spring are substantially lower as compared to mid-summer, in particular at bloom sites (Christaki *et al*., 2014). In contrast to the present study, total and active prokaryotic communities were different from each other in summer, both within the phytoplankton bloom above the Kerguelen plateau (Station A3) and in HNLC waters (West *et al*., 2008). These observations suggest that while prokaryotes are stimulated by phytoplankton growth in early spring, our approach does not allow to differentiate the active community members from those potentially inactive or dormant (Lennon and Jones, 2011).

Our observation that key diatom species are each associated to several distinct prokaryotic taxa raises the question on the underlying mechanisms. While the exact processes are not tractable with the present data set, we provide a possible scenario. In contrast to heterotrophic prokaryotes, the spatial distribution of diatoms was significantly correlated to some environmental parameters. Because our study took place in early spring when the effect of phytoplankton activity on inorganic nutrient drawdown is minor, this result suggests that environmental parameters are drivers of diatom assemblages, and that diatoms may be setting the pace for the observed spatial changes in prokaryotic community composition. Previous field studies and satellite observations have indicated that the onset of spring phytoplankton blooms occurring in the region off Kerguelen Island can differ by several weeks (Sallée *et al*., 2015). Considering each site independently, the varying contributions of the most abundant diatom species could represent different stages of the spring phytoplankton development at a given location with potential consequences on the prokaryotic community composition. The

qualitative and quantitative differences in the DOM produced by the various diatoms are likely to present an important selection process (Landa *et al*., 2016; Sarmento *et al*., 2016).

The pronounced association between assemblages of diatoms and heterotrophic microbes observed in the present study could be driven by two particular features of the Southern Ocean that are the growth-limiting concentrations of bioavailable iron and organic carbon in surface waters. Iron availability controls autotrophic and heterotrophic metabolism, but the lack of bioavailable organic carbon represents an additional constraint for heterotrophic microbes (Church *et al*., 2000; Obernosterer *et al*., 2015). In early spring, autotrophic plankton outcompete heterotrophs for the access to iron (Fourquez *et al*., 2015). Thus, diatom-derived organic matter is key in driving both heterotrophic microbial activity and diversity in this ocean region (Arrieta *et al*., 2004; Obernosterer *et al*., 2008; Landa *et al*., 2016; Luria *et al*., 2016). The spatial distribution of the diatom assemblages as observed in the present study in early spring likely reflects their respective ecological niches driven by the light-nutrient regime, including iron availability. Our results let us conclude that diatom assemblages shape the habitat type for heterotrophic microbes and thereby directly influence their community composition.

Experimental procedures

Study area and sampling strategy

The present study was performed during the Southern Ocean and Climate (SOCLIM) cruise (DOI:10.17600/16003300) aboard the *R/V Marion Dufresne* (October 08 to November 1 2016). The 12 stations sampled for the present study were located in four oceanographic

zones, the subtropical zone (STZ), the subantarctic zone (SAZ), the polar front zone (PFZ), and the antarctic zone (AAZ) (Fig. 1; Table 1). In the AAZ, station A3, located above the Kerguelen plateau, was visited twice during the sampling period (stations A3-1 and A3-2). Station BDT (Baie de la Table) is a coastal site (50m overall depth) within a bay of Kerguelen Island. All environmental data and the samples for the diatom community composition were collected at 10m with 12L Niskin bottles mounted on a rosette equipped with a conductivity-temperature-depth (CTD, Seabird SBE9+) sensor. Seawater samples for microbial diversity analyses were taken from the underway seawater supply system that collected water at 5m depth.

The sampling, storage and analyses of common environmental parameters were done according to previously described protocols. The major inorganic nutrients nitrite (NO_2^-), nitrate (NO_3^-), phosphate (PO_4^{3-}) and silicic acid ($Si(OH)_4$) were determined using continuous flow analysis with a Skalar instrument (Aminot, 2007; Blain *et al*., 2014). Dissolved organic carbon (DOC) concentrations were determined by high temperature oxydation on a Shimadzu TOC-VCP analyser (Benner and Strom 1993; Obernosterer *et al*., 2015). Concentrations of chlorophyll *a* (Chl *a*) were determined by High Performance Liquid Chromatography (HPLC) analyses (Uitz *et al*., 2009). The abundance of heterotrophic and autotrophic prokaryotes, and pico-and nanoeukaryotes was done by flow cytometric analyses on a BD FACS canto (Marie *et al*., 2000; Obernosterer *et al*., 2008). For the identification and enumeration of the diatom and dinoflagellate assemblages, 100 mL of seawater were fixed with Lugol solution (1 % final concentration) and stored in the dark at 4°C for 2 months. Observations were done in an Utermöhl counting chamber (24h, dark) using an inverted microscope with phase contrast (Olympus IX70) with x400 magnification as described in Rembauville et al. (2017).

For the analyses of the prokaryotic community composition, three 6L biological replicates were collected at each site, filtered on 60 µm nylon screens, and then through 0.8

µm polycarbonate filters (47-mm diameter, Nuclepore, Whatman, Sigma Aldrich, St Louis, MO, USA). Cells were then concentrated on 0.2 µm Sterivex filter units (Sterivex, Millipore, EMD, Billerica, MA, USA) using a peristaltic pumping system (Masterflex L/S Easy-Load II). The Sterivex filter units were kept at -80 °C until extraction.

DNA and RNA extraction and sequencing preparation

DNA and RNA were simultaneously extracted from one Sterivex filter unit using the AllPrep DNA /RNA kit (Qiagen, Hiden, Germany) with the following modifications. Filter units were thawed and closed with a sterile pipette tip end at the outflow. Lysis buffer was added (40 mM EDTA, 50 mM Tris, 0.75 M sucrose) and 3 freeze and thaw cycles were performed using liquid nitrogen and a water bath at 65 °C. Lysozyme solution (0.2 mg ml^{-1} final concentration) was added and filter units were placed on a rotary mixer at 37°C for 45 minutes. Proteinase K (0.2 mg ml^{-1} final concentration) and SDS (1% final concentration) were added and filter units were incubated at 55 °C with gentle agitation every 10 minutes for 1 hour. To protect the RNA, 10 µl of *β*-mercaptoethanol was added to 1 ml of RLT plus buffer provided by the kit. To each filter unit, 1550 µl RLT plus-*β*-mercaptoethanol was added and inverted to mix. The lysate was recovered by using a sterile 5 ml syringe and loaded in three additions onto the DNA columns by centrifuging at 10,000 g for 30 seconds. DNA and RNA purification were performed following manufacturer's guidelines (Qiagen, Germany) in which RNA was treated with DNase to avoid DNA contamination after the first wash step.

RNA was converted to cDNA using SuperScript III Reverse Transcriptase according to the manufacturer's instructions. Prior to reverse transcription, quality of RNA samples was examined by PCR test with general primer sets 341F (5' - CCTACGGGNGGCWGCAG) and 805R (5'- GACTACHVGGGTATCTAATCC) for the prokaryotic 16S rRNA gene, followed

by the examination of amplification products on 1% agarose electrophoresis. Based on the results of the PCR test, DNase was performed once more on the RNA extracts of those samples with contaminating DNA left, to completely remove the residual DNA. DNA and cDNA was amplified and pooled as described in Parada et al. (2016) with a modification to the PCR amplification step. Briefly, the V4 - V5 region of the 16S rRNA gene from DNA and cDNA samples was amplified with the primer sets 515F-Y (5' - GTGYCAGCMGCCGCGGTAA) and 926R (5' - CCGYCAATTYMTTTRAGTTT). Triplicate 10 µl reaction mixtures contained 2 µg DNA, 5 µl KAPA2G Fast HotStart ReadyMix, 0.2 µM forward primer and 0.2 µM reverse primer. Cycling reaction started with a 3min heating step at 95 °C followed by 22 cycles of 95 °C for 45 s, 50 °C for 45 s, 68 °C for 90 s, and a final extension of 68 °C for 5 min. The presence of amplification products was confirmed by 1 % agarose electrophoresis and triplicate reactions were pooled. Each sample were added with unique paired barcodes. The Master 25 µl mixtures contained 1 µl PCR product, 12.5 µl KAPA2G Fast HotStart ReadyMix (Kapa Biosystems, USA), 0.5 µl barcode 1 and 0.5 µl barcode 2. The cycling program included a 30 s initial denaturation at 98°C followed by 8 cycles of 98 °C for 10 s, 60 °C for 20 s, 72 °C for 30 s, and a final extension of 72 °C for 2 min. 3 µl PCR product were used to check for amplification on 1% agarose electrophoresis. The remaining 22 µl barcoded amplicon product was cleaned to remove unwanted dNTPs and primers by Exonuclease I and Shrimp Alkaline Phosphatase at 37 °C, 30 min for treatment and 85 °C, 15 min to inactivate. The concentration of double-stranded DNA was quantified by PicoGreen fluorescence assay (Life Technologies). After calculating the PCR product concentration of each samples, they were pooled at equal concentrations manually. The pooled PCR amplicons were concentrated using Wizard SV gel and PCR clean-up system (Promega, USA) according to the manufacturer's protocol. 16S rRNA gene amplicons were sequenced with Illumina MiSeq 2 x 300 bp chemistry on one flow-cell at

Fasteris SA sequencing service (Switzerland). Mock community DNA (LGC standards, UK) was used as a standard for subsequent analyses and considered as a DNA sample for all treatments.

Data analysis

All samples from the same sequencing run have been demultiplexed by Fasteris SA and barcodes have been trimmed off. A total number of 4 150 902 sequences was obtained. Processing of sequences were performed using the Usearch pipeline (Edgar, 2013). Paired-end reads were merged using *fastq-mergepairs*. The positions of primers were checked using *search_oligodb* and *fastx_subsample* were used to subset a portion of all sequences to check (e.g. 5000 sequences). Primers were trimmed and merged reads in range of length from 336 to 486 were kept using *fastq-filter* based on maximum expected error (Needham and Fuhrman, 2016). 2 000 219 sequences were kept after quality filtering. Data were denoised and chimera were identified and removed using *unoise3* with a *minsize* 10 according to mock community DNA (Edgar, 2016). During this step, singletons were discarded. Sequences were clustered using *usearch_global* and defined as OTUs at a 97% sequence similarity level. OTUs were assigned using *assign_taxonomy.py* against SILVA release 132 database (Quast *et al.*, 2012). Sequences assigned to chloroplast were removed prior to subsequent analyses.

Statistical analyses

All statistical analyses were performed using R 3.4.2 version. The OTU and taxa tables were combined into one object using phyloseq R package.

Data were Hellinger transformed prior to the analyses based on Bray-Curtis dissimilarity (Legendre and Gallagher, 2001). Bray-Curtis dissimilarity matrices were generated via *vegdist()* function. Non-metric dimensional scaling (NMDS) ordinations was generated based on Bray-Curtis dissimilarity using *monoMDS()* function in the package Vegan (Oksanen *et al*., 2015). Analysis of similarity (ANOSIM) was performed to test significant differences between sampling zones in microbial communities with R. Dendrograms were performed using *hclust()* with method "average" in the Vegan package.

Mantel and partial Mantel tests were performed in Vegan using *mantel()* and *mantel.partial()* based on the Pearson correlation method. The linear model was applied for the relationship between prokaryotic communities versus diatom communities in R. Geographical coordinates were transformed using the Haversine formula (Sinnott, 1984). Prior to correlation analysis, environmental variables were z-score transformed. The amount of variance in prokaryotic community composition explained by diatoms were estimated as the square of the correlation coefficient (Rho^2) based on partial Mantel test.

Sequences alignment was carried out using MAFFT algorithm web services by defaults (Katoh *et al*., 2017). The phylogenetic tree was constructed using PhyML 3.0 online programs based on maximum likelihood method and 100 bootstraps with HKY85 substitution model (Guindon and Gascuel, 2003). The tree was visualized with SeaView version 4.7 and saved as rooted tree. Heat maps were generated using heatmap3 package and rows were reordered corresponding to phylogenetic tree. The correlation heatmaps were generated using *spls()* and *cim()* in the mixOmics package with log-transformed data (Chun and Keleş, 2010; Rohart *et al*., 2017).

Canonical correspondance analysis were performed using *cca()* in Vegan package with z-score transformed data. The significance of environmental parameters was tested with an analysis of variance (ANOVA) using Vegan package in R.

Accession numbers

Demultiplexed sequence files are available in NCBI under accession number PRJNA494099.

Conflict of interest

The authors declare no conflict of interest.

Acknowledgments

We thank the captain and the crew of the *R/V Marion Dufresne* for their support aboard. We thank Olivier Crispi for sampling and analyses of inorganic nutrients, Jocelyne Caparros for the analyses of dissolved organic carbon and Philippe Catala for flow cytometry analyses. Chlorophyll *a* concentrations were determined by HPLC analyses at the SAPIGH analytical platform at IMEV, Villefranche-sur-Mer, by Josefine Ras and Celine Dimier. The detailed comments from two anonymous reviewers helped improve previous versions of the manuscript. The project SOCLIM (Southern Ocean and Climate) is supported by the Climate Initiative of the BNP Paribas foundation, the French Polar Institute (Institut Polaire Emile Victor), and the French program LEFE-CYBER of the CNRS-INSU. This work is part of the PhD thesis of Y.L. supported by the China Scholarship Council (CSC; NO. 201606330072).

References

Amin, S.A., Green, D.H., Hart, M.C., Kupper, F.C., Sunda, W.G., and Carrano, C.J. (2009) Photolysis of iron-siderophore chelates promotes bacterial-algal mutualism. *Proc Natl Acad Sci USA* **106**: 17071–17076.

Amin, S.A., Hmelo, L.R., van Tol, H.M., Durham, B.P., Carlson, L.T., Heal, K.R., *et al*. (2015) Interaction and signalling between a cosmopolitan phytoplankton and associated bacteria. *Nature* **522**: 98–101.

Amin, S.A., Parker, M.S., and Armbrust, E.V. (2012) Interactions between diatoms and bacteria. *Microbiol Mol Biol Rev* **76**: 667–684.

Aminot, A. and Kérouel, R. (2007) Dosage automatique des nutriments dans les eaux marines: méthodes en flux continu. Editions Quae.

Arrieta, J.M., Weinbauer, M.G., Lute, C., and Herndl, G.J. (2004) Response of bacterioplankton to iron fertilization in the Southern Ocean. *Limnol Oceanogr* **49**: 799–808.

Assmy, P., Smetacek, V., Montresor, M., Klaas, C., Henjes, J., Strass, V.H., *et al*. (2013) Thick-shelled, grazer-protected diatoms decouple ocean carbon and silicon cycles in the iron-limited Antarctic Circumpolar Current. *Proc Natl Acad Sci USA* **110**: 20633–20638.

Beier, S., Rivers, A.R., Moran, M.A., and Obernosterer, I. (2015) The transcriptional response of prokaryotes to phytoplankton-derived dissolved organic matter in seawater: The response of prokaryotes to DOM in seawater. *Environ Microbiol* **17**: 3466–3480.

Benner, R. and Strom, M. (1993) A critical evaluation of the analytical blank associated with DOC measurements by high-temperature catalytic oxidation. *Marine Chemistry* **41**:

153–160.

Biddanda, B. and Benner, R. (1997) Major contribution from mesopelagic plankton to heterotrophic metabolism in the upper ocean. *Deep Sea Res Part 2 Oceanogr Res Pap* **44**: 2069–2085.

Blain, S., Capparos, J., Guéneuguès, A., Obernosterer, I., and Oriol, L. (2014) Distributions and stoichiometry of dissolved nitrogen and phosphorus in the iron fertilized region near Kerguelen (Southern Ocean). *Biogeosciences Discussions* **11**: 9949–9977.

Blain, S., Quéguiner, B., Armand, L., Belviso, S., Bombled, B., Bopp, L., *et al*. (2007) Effect of natural iron fertilization on carbon sequestration in the Southern Ocean. *Nature* **446**: 1070–1074.

Blazewicz, S.J., Barnard, R.L., Daly, R.A., and Firestone, M.K. (2013) Evaluating rRNA as an indicator of microbial activity in environmental communities: limitations and uses. *ISME J* **7**: 2061–2068.

Buchan, A., LeCleir, G.R., Gulvik, C.A., and González, J.M. (2014) Master recyclers: features and functions of bacteria associated with phytoplankton blooms. *Nat Rev Microbiol* **12**: 686–698.

Bunse, C. and Pinhassi, J. (2017) Marine bacterioplankton seasonal succession dynamics. *Trends Microbiol* **25**: 494–505.

Christaki, U., Lefèvre, D., Georges, C., Colombet, J., Catala, P., Courties, C., *et al*. (2014) Microbial food web dynamics during spring phytoplankton blooms in the naturally iron-fertilized Kerguelen area (Southern Ocean). *Biogeosciences* **11**: 6739–6753.

Chun, H. and Keleş, S. (2010) Sparse partial least squares regression for simultaneous

dimension reduction and variable selection. *J Roy Stat Society: Series B (Stat Met)* **72**: 3–25.

Church, M.J., Hutchins, D.A. and Ducklow, H.W. (2000) Limitation of bacterial growth by dissolved organic matter and iron in the Southern Ocean. *Appl Environ Microb* **66**: 455-466.

Ciais, P., C. Sabine, G. Bala, L. Bopp, V. Brovkin, J. Canadell, *et al*. (2014) Carbon and Other Biogeochemical Cycles. In *Climate Change 2013*: The Physical Science Basis. Contribution of Working Group I to the Fifth Assessment Report of the Intergovernmental Panel on Climate Change. Stocker, T.F., D. Qin, G.-K. Plattner, M. Tignor, S.K. Allen, J. Boschung, *et al*. (eds). Cambridge: Cambridge University Press, pp. 465-570.

Dadaglio, L., Dinasquet, J., Obernosterer, I., and Joux, F. (2018) Differential responses of bacteria to diatom-derived dissolved organic matter in the Arctic Ocean. *Aquat Microb Ecol* **82**: 59–72.

Delmont, T.O., Hammar, K.M., Ducklow, H.W., Yager, P.L., and Post, A.F. (2014) *Phaeocystis antarctica* blooms strongly influence bacterial community structures in the Amundsen Sea polynya. *Front Microbiol* **5**: 646.

Dinasquet, J., Richert, I., Logares, R., Yager, P., Bertilsson, S., and Riemann, L. (2017) Mixing of water masses caused by a drifting iceberg affects bacterial activity, community composition and substrate utilization capability in the Southern Ocean: Iceberg influence on bacterioplankton. *Environ Microbiol* **19**: 2453–2467.

Ducklow, H.W., Fraser, W., Karl, D.M., Quetin, L.B., Ross, R.M., Smith, R.C., *et al*. (2006) Water-column processes in the West Antarctic Peninsula and the Ross Sea:

Interannual variations and foodweb structure. *Deep Sea Res Part 2 Top Stud in Oceanogr* **53**: 834–852.

Durham, B.P., Sharma, S., Luo, H., Smith, C.B., Amin, S.A., Bender, S.J., *et al*. (2015) Cryptic carbon and sulfur cycling between surface ocean plankton. *Proc Natl Acad Sci USA* **112**: 453–457.

Edgar, R.C. (2013) UPARSE: highly accurate OTU sequences from microbial amplicon reads. *Nat Methods* **10**: 996–998.

Edgar, R.C. (2016) UNOISE2: improved error-correction for Illumina 16S and ITS amplicon sequencing. *BioRxiv* 081257.

Fegatella, F., Lim, J., Kjelleberg, S., and Cavicchioli, R. (1998) Implications of rRNA Operon Copy Number and Ribosome Content in the Marine Oligotrophic Ultramicrobacterium *Sphingomonas* sp. Strain RB2256. *Appl Environ Microb* **64**: 6.

Flärdh, K., Cohen, P.S., and Kjelleberg, S. (1992) Ribosomes exist in large excess over the apparent demand for protein synthesis during carbon starvation in marine *Vibrio* sp. strain CCUG 15956. *J Bacteriol* **174**: 6780–6788.

Fourquez, M., Obernosterer, I., Davies, D.M., Trull, T.W. and Blain, S. (2015) Microbial iron uptake in the naturally fertilized waters in the vicinity of the Kerguelen Islands: phytoplankton–bacteria interactions. *Biogeosciences*, **12:** 1893-1906.

Gilbert, J.A., Steele, J.A., Caporaso, J.G., Steinbrück, L., Reeder, J., Temperton, B., *et al*. (2012) Defining seasonal marine microbial community dynamics. *ISME J* **6**: 298–308.

Guindon, S. and Gascuel, O. (2003) A simple, fast, and accurate algorithm to estimate large phylogenies by maximum likelihood. *Syst Biol* **52**: 696–704.

Hanson, C.A., Fuhrman, J.A., Horner-Devine, M.C., and Martiny, J.B.H. (2012) Beyond biogeographic patterns: processes shaping the microbial landscape. *Nat Rev Microbiol* **10**: 497–506.

Johnson, W.M., Kido Soule, M.C., and Kujawinski, E.B. (2016) Evidence for quorum sensing and differential metabolite production by a marine bacterium in response to DMSP. *ISME J* **10**: 2304–2316.

Katoh, K., Rozewicki, J., and Yamada, K.D. (2017) MAFFT online service: multiple sequence alignment, interactive sequence choice and visualization. *Brief Bioinform*.

Kerkhof, L. and Ward, B.B. (1993) Comparison of Nucleic Acid Hybridization and Fluorometry for Measurement of the Relationship between RNA/DNA Ratio and Growth Rate in a Marine Bacterium. **59**: 7.

Klindworth, A., Mann, A.J., Huang, S., Wichels, A., Quast, C., Waldmann, J., *et al*. (2014) Diversity and activity of marine bacterioplankton during a diatom bloom in the North Sea assessed by total RNA and pyrotag sequencing. *Marine genomics* **18**:185-192.

Landa, M., Blain, S., Christaki, U., Monchy, S., and Obernosterer, I. (2016) Shifts in bacterial community composition associated with increased carbon cycling in a mosaic of phytoplankton blooms. *ISME J* **10**: 39–50.

Lasbleiz, M., Leblanc, K., Armand, L.K., Christaki, U., Georges, C., Obernosterer, I., and Quéguiner, B. (2016) Composition of diatom communities and their contribution to plankton biomass in the naturally iron-fertilized region of Kerguelen in the Southern Ocean. *FEMS Microbiol Ecol* **92**: fiw171.

Legendre, P. and Gallagher, E. (2001) Ecologically meaningful transformations for ordination of species data. *Oecologia* **129**: 271–280.

Lennon, J. T. and Jones, S. E. (2011) Microbial seed banks: the ecological and evolutionary implications of dormancy. *Nat Rev Microbiol* **9**: 119.

Li, D.-X., Zhang, H., Chen, X.-H., Xie, Z.-X., Zhang, Y., Zhang, S.-F., *et al*. (2018) Metaproteomics reveals major microbial players and their metabolic activities during the blooming period of a marine dinoflagellate *Prorocentrum donghaiense*: Microbial metaproteome during a dinoflagellate bloom. *Environ Microbiol* **20**: 632–644.

Lima-Mendez, G., Faust, K., Henry, N., Decelle, J., Colin, S., Carcillo, F., *et al*. (2015) Determinants of community structure in the global plankton interactome. *Science* **348**: 1262073–1262073.

Lindström, E.S. and Langenheder, S. (2012) Local and regional factors influencing bacterial community assembly: Bacterial community assembly. *Environ Microbiol Rep* **4**: 1–9.

Luria, C.M., Amaral-Zettler, L.A., Ducklow, H.W., Repeta, D.J., Rhyne, A.L., and Rich, J.J. (2017) Seasonal shifts in bacterial community responses to phytoplankton-derived dissolved organic matter in the Western Antarctic Peninsula. *Front Microbiol* **8**: 2117.

Luria, C.M., Amaral-Zettler, L.A., Ducklow, H.W., and Rich, J.J. (2016) Seasonal succession of free-living bacterial communities in coastal waters of the Western Antarctic Peninsula. *Front Microbiol* **7**: 1731.

Malviya, S., Scalco, E., Audic, S., Vincent, F., Veluchamy, A., Poulain, J., *et al*. (2016) Insights into global diatom distribution and diversity in the world's ocean. *Proc Natl Acad Sci USA* **113**: E1516–E1525.

Marie, D., Simon, N., Guillon, L., Partensky, F., and Vaulot, D. (2000) Flow cytometry analysis of marine picoplankton. In *Living Color*: Protocols in flow cytometry and cell sorting. Maggio, D. (ed). Berlin, Heidelberg: Springer, pp. 421–454.

Milici, M., Deng, Z.-L., Tomasch, J., Decelle, J., Wos-Oxley, M.L., Wang, H., *et al*. (2016) Co-occurrence Analysis of Microbial Taxa in the Atlantic Ocean Reveals High Connectivity in the Free-Living Bacterioplankton. *Front Microbiol* **7**: 649.

Myklestad, S.M. (2000) Dissolved organic carbon from phytoplankton. In *Marine Chemistry*. Wangersky, P.J. (ed). Berlin, Heidelberg: Springer, pp. 111–148.

Needham, D.M. and Fuhrman, J.A. (2016) Pronounced daily succession of phytoplankton, archaea and bacteria following a spring bloom. *Nat Microbiol* **1**: 16005.

Obernosterer, I., Christaki, U., Lefèvre, D., Catala, P., Van Wambeke, F., and Lebaron, P. (2008) Rapid bacterial mineralization of organic carbon produced during a phytoplankton bloom induced by natural iron fertilization in the Southern Ocean. *Deep Sea Res Part 2 Top Stud in Oceanogr* **55**: 777–789.

Obernosterer, I., Fourquez, M., and Blain, S. (2015) Fe and C co-limitation of heterotrophic bacteria in the naturally fertilized region off the Kerguelen Islands. *Biogeosciences* **12**: 1983–1992.

Oksanen, J., Blanchet, F.G., Kindt, R., Legendre, P., Minchin, P.R., O'Hara, *et al*. (2015) vegan: community ecology package. R package version 2.3–0.

Paerl, R.W., Bouget, F.-Y., Lozano, J.-C., Vergé, V., Schatt, P., Allen, E.E., *et al*. (2017) Use of plankton-derived vitamin B1 precursors, especially thiazole-related precursor, by key marine picoeukaryotic phytoplankton. *ISME J* **11**: 753–765.

Parada, A.E., Needham, D.M., and Fuhrman, J.A. (2016) Every base matters: assessing small subunit rRNA primers for marine microbiomes with mock communities, time series and global field samples: Primers for marine microbiome studies. *Environ Microbiol* **18**: 1403–1414.

Poulsen, L. K., Ballard, G., and Stahl, D. A. (1993). Use of rRNA fluorescence in situ hybridization for measuring the activity of single cells in young and established biofilms. *Appl Environ Microb*, **59**: 1354-1360.

Quast, C., Pruesse, E., Yilmaz, P., Gerken, J., Schweer, T., Yarza, P., *et al*. (2012) The SILVA ribosomal RNA gene database project: improved data processing and web-based tools. *Nucleic Acids Res* **41**: D590–D596.

Quéguiner, B. (2013) Iron fertilization and the structure of planktonic communities in high nutrient regions of the Southern Ocean. *Deep Sea Res Part 2 Top Stud in Oceanogr* **90**: 43–54.

Rembauville, M., Briggs, N., Ardyna, M., Uitz, J., Catala, P., Penkerc'h, C., *et al*. (2017) Plankton assemblage estimated with BGC-Argo Floats in the Southern Ocean: Implications for seasonal successions and particle export. *J Geophys Res: Oceans* **122**: 8278–8292.

Rinta-Kanto, J.M., Sun, S., Sharma, S., Kiene, R.P., and Moran, M.A. (2012) Bacterial community transcription patterns during a marine phytoplankton bloom: Phytoplankton bloom metatranscriptome. *Environ Microbiol* **14**: 228–239.

Rohart, F., Gautier, B., Singh, A., and Lê Cao, K.-A. (2017) mixOmics: An R package for 'omics feature selection and multiple data integration. *PLOS Comput Biol* **13**: e1005752.

Sallée, J.-B., Llort, J., Tagliabue, A., and Lévy, M. (2015) Characterization of distinct bloom phenology regimes in the Southern Ocean. *ICES J Marine Science: Journal du Conseil* **72**: 1985–1998.

Sarmento, H. and Gasol, J.M. (2012) Use of phytoplankton-derived dissolved organic carbon

by different types of bacterioplankton: Use of phytoplankton-derived DOC by bacterioplankton. *Environ Microbiol* **14**: 2348–2360.

Sarmento, H., Morana, C., and Gasol, J.M. (2016) Bacterioplankton niche partitioning in the use of phytoplankton-derived dissolved organic carbon: quantity is more important than quality. *ISME J* **10**: 2582–2592.

Sheik, C.S., Jain, S., and Dick, G.J. (2014) Metabolic flexibility of enigmatic SAR324 revealed through metagenomics and metatranscriptomics: Disentangling the ecophysiological role of SAR324. *Environ Microbiol* **16**: 304–317.

Sinnott, R.W. (1984) Virtues of the Haversine. *Sky Telesc* **68**: 158.

Smetacek, V., Assmy, P., and Henjes, J. (2004) The role of grazing in structuring Southern Ocean pelagic ecosystems and biogeochemical cycles. *Antarct Sci* **16**: 541–558.

Sowell, S.M., Wilhelm, L.J., Norbeck, A.D., Lipton, M.S., Nicora, C.D., Barofsky, D.F., *et al*. (2009) Transport functions dominate the SAR11 metaproteome at low-nutrient extremes in the Sargasso Sea. *ISME J* **3**: 93–105.

Swan, B.K., Martinez-Garcia, M., Preston, C.M., Sczyrba, A., Woyke, T., Lamy, D., *et al*. (2011) Potential for chemolithoautotrophy among ubiquitous bacteria lineages in the Dark Ocean. *Science* **333**: 1296–1300.

Swan, B.K., Tupper, B., Sczyrba, A., Lauro, F.M., Martinez-Garcia, M., Gonzalez, J.M., *et al*. (2013) Prevalent genome streamlining and latitudinal divergence of planktonic bacteria in the surface ocean. *Proc Natl Acad Sci USA* **110**: 11463–11468.

Tada, Y., Nakaya, R., Goto, S., Yamashita, Y., and Suzuki, K. (2017) Distinct bacterial community and diversity shifts after phytoplankton-derived dissolved organic matter

addition in a coastal environment. *J Exp Mar Biol Ecol* **495**: 119–128.

Teeling, H., Fuchs, B.M., Becher, D., Klockow, C., Gardebrecht, A., Bennke, C.M., *et al*. (2012) Substrate-controlled succession of marine bacterioplankton populations induced by a phytoplankton bloom. *Science* **336**: 608–611.

Thompson, A.W., Foster, R.A., Krupke, A., Carter, B.J., Musat, N., Vaulot, D., *et al*. (2012) Unicellular cyanobacterium symbiotic with a single-celled eukaryotic alga. *Science* **337**: 1546–1550.

Uitz, J., Claustre, H., Griffiths, F.B., Ras, J., Garcia, N. and Sandroni, V. (2009) A phytoplankton class-specific primary production model applied to the Kerguelen Islands region (Southern Ocean). *Deep Sea Res Part 1 Oceanogr Res Pap* **56:** 541-560.

van Tol, H.M., Amin, S.A., and Armbrust, E.V. (2017) Ubiquitous marine bacterium inhibits diatom cell division. *ISME J* **11**: 31–42.

West, N.J., Obernosterer, I., Zemb, O., and Lebaron, P. (2008) Major differences of bacterial diversity and activity inside and outside of a natural iron-fertilized phytoplankton bloom in the Southern Ocean. *Environ Microbiol* **10**: 738–756.

Wilkins, D., van Sebille, E., Rintoul, S.R., Lauro, F.M., and Cavicchioli, R. (2013) Advection shapes Southern Ocean microbial assemblages independent of distance and environment effects. *Nat Communications* **4**: 2457.

Williams, T.J., Wilkins, D., Long, E., Evans, F., DeMaere, M.Z., Raftery, M.J., and Cavicchioli, R. (2013) The role of planktonic *Flavobacteria* in processing algal organic matter in coastal East Antarctica revealed using metagenomics and metaproteomics: Metaproteomics of marine Antarctic *Flavobacteria*. *Environ Microbiol* **15**: 1302–1317.

Yooseph, S., Nealson, K.H., Rusch, D.B., McCrow, J.P., Dupont, C.L., Kim, M., *et al*. (2010) Genomic and functional adaptation in surface ocean planktonic prokaryotes. *Nature* **468**: 60–66.

Zehr, J.P. (2015) How single cells work together. *Science* **349**: 1163–1164.

Zhou, J., Song, X., Zhang, C.-Y., Chen, G.-F., Lao, Y.-M., Jin, H., and Cai, Z.-H. (2018) Distribution Patterns of Microbial Community Structure Along a 7000-Mile Latitudinal Transect from the Mediterranean Sea Across the Atlantic Ocean to the Brazilian Coastal Sea. *Microbial Ecology* **76**: 592–609.

Table Legends

Table 1. Brief description of the study sites. All values are from 10m depth.

Table 2. Partial Mantel test for prokaryotic and diatom community composition and geographic distance (a) and combined environmental parameters (b) for Southern Ocean samples.

The values shown in the tables are Rho values. Each value represents the correlation between two matrices while controlling for the effect of the third matrix. ** $P < 0.01$, * $P < 0.05$

Figure Legends

Fig. 1. Map of the study region of the Southern Ocean and Climate (SOCLIM) cruise (October 2016) with stations sampled for the present study indicated by white dots. Surface chlorophyll *a* is derived from ocean color satellite images (COPERNICUS-GLOBCOLOR, October 2016, resolution 25km). Dotted and full lines indicate ocean zones and fronts, respectively. STZ-Subtropical Zone, STF- Subtropical Front, SAZ-Subantarctic Zone, SAF-Subantarctic Front, PFZ-Polar Front Zone, PF-Polar Front, AAZ-Antarctic Zone.

Fig. 2. Clustering of stations based on Bray-Curtis dissimilarity of the diatom community composition and relative abundances of diatom species. Diatom species with a relative abundance ≥ 1% in at least one station are shown. Samples from the 4 ocean zones were significantly different (ANOSIM, $R = 0.78$, $P < 0.01$). STZ-Subtropical Zone, SAZ-Subantarctic Zone, PFZ-Polar Front Zone, AAZ-Antarctic Zone. Note: color codes and associated names are ordered from top to bottom of each panel.

Fig. 3. Non-metric multidimensional scaling (NMDS) of total (DNA) and active (RNA) prokaryotic communities based on Bray-Curtis dissimilarity. Biological replicates of total and active prokaryotic communities are shown for each station. Samples from the 4 ocean zones were significantly different (2D stress = 0.08; ANOSIM, $R = 0.69$, $P < 0.01$). STZ-Subtropical Zone, SAZ-Subantarctic Zone, PFZ-Polar Front Zone, AAZ-Antarctic Zone.

Fig. 4. Relationship between changes in the community composition of diatoms and of total prokaryotes for the Southern Ocean stations (SAZ, PFZ and AAZ excluding station BDT). Each point represents the Bray-Curtis dissimilarity between pairs of samples. The correlation coefficient was determined by the Mantel test. Dashed line denotes linear regression.

Fig. 5. Heatmap of correlations between dominant diatom species and prokaryotic OTUs from total communities based on Pearson correlations. Diatom species and prokaryotic OTUs with ≥ 1% relative abundance in at least one sample are shown. Colour key: Red and blue colours represent positive and negative correlations, respectively. a.t = ambiguous taxa

Supporting information

Additional Supporting Information may be found in the online version of this article:

Fig. S1. Dendrograms of total (a) and active (b) prokaryotic communities based on Bray-Curtis dissimilarity of biological triplicates. Triplicates were named with number of station followed by a, b and c.

Fig. S2. Heatmap and phylogenetic tree of dominant prokaryotic OTUs that account for ≥ 1% in at least one sample of the total (a) or active (b) prokaryotic community. The taxonomy classification of each OTU was done according to their closest sequence match assigned by the SILVA database.

Colour key: dark red and light yellow colours represent high and low abundances, respectively. a.t = ambiguous taxa

Fig. S3. Relationship between changes in the community composition of diatoms and of active prokaryotes. Each point represents the Bray-Curtis dissimilarity between pairs of samples. The correlation coefficient was determined by the Mantel test. Dashed lines denote linear regressions for the Southern Ocean stations (SAZ, PFZ and AAZ excluding station BDT).

Fig. S4. Relationship between changes in prokaryotic and diatom communities. Each point represents the Bray-Curtis dissimilarity between pairs of samples. The correlation coefficients were determined by Mantel test. (a) Total prokaryotic communities. The full line denotes the linear regression across the entire transect (filled and empty circles combined). The dashed line denotes the linear regression across the Southern Ocean (SAZ, PFZ and AZ excluding sample BDT) regions (empty circles only). (b) Active prokaryotic communities. The full line denotes the linear regression across the entire transect (filled and empty squares combined).

The dashed line denotes the linear regression across the Southern Ocean (SAZ, PFZ and AZ excluding sample BDT) regions (empty squares only).

Fig. S5. Distance-decay curves of dissimilarity of the composition of the total prokaryotic communities. Each point represents the Bray-Curtis dissimilarity between pairs of samples. The correlation coefficients were determined by Mantel test. (a) entire transect (b) Southern Ocean (SAZ, PFZ and AZ excluding sample BDT). Non-significant results were also obtained for the active prokaryotic communities (data not shown).

Fig. S6. Canonical correspondence analysis of prokaryotic community composition and environmental parameters for (a) the entire transect and (b) for the Southern Ocean (SAZ, PFZ and AZ excluding sample BDT). Highly auto-correlated parameters are not shown (PO_4^{3-} with NO_3^- and dissolved oxygen with temperature). The significant parameters were temperature, salinity and DOC for the entire transect (a) and temperature for the Southern Ocean (b). Station BDT was not considered because chlorophyll *a* data was not available.

Table S1. Additional environmental variables of the study sites.

Table S2. Partial Mantel test for prokaryotic and diatom community composition and geographic distance (a) and environmental parameters (b) for the entire dataset and Southern Ocean samples.

Table 1. Brief description of the study sites. All values are from 10m depth.

Station	Date	Lat/ Long	Temp (°C)	∑N (µM)	PO_4^{3-} (µM)	$Si(OH)_4$ (µM)	DOC (µM)	Chl *a* ($\mu g\ L^{-1}$)	BA ($x10^8 L^{-1}$)	Synecho ($x10^4 L^{-1}$)	PicoNano ($x\ 10^6 L^{-1}$)	Diatoms ($x\ 10^4 L^{-1}$)	Dinoflag ($x\ 10^4 L^{-1}$)
Subtropical Zone													
O22	08-Oct-16	29.00°S 58.93°E	20.09	0.04	0.04	1.75	76	0.06	5.51	170.0	1.13	0.24	1.96
O24	10-Oct-16	38.00°S 63.65°E	14.60	2.91	0.21	2.37	62	0.29	7.64	3160.0	12.07	14.75	3.55
Subantarctic Zone													
O25	12-Oct-16	45.00°S 67.77°E	7.61	19.06	1.25	2.03	51	0.42	5.05	902.0	9.65	63.20	1.55
Polar Front Zone													
O12	25-Oct-16	47.00°S 72.22°E	4.60	25.42	1.68	7.72	50	0.39	6.02	134.0	4.79	14.52	3.44
TNS6	15-Oct-16	48.78°S 72.28°E	2.92	26.51	1.93	13.93	52	1.02	3.94	57.4	3.86	64.40	11.40
BDT	17-Oct-16	49.50°S 69.21°E	2.94	26.30	1.81	14.29	68	n.a	4.46	47.7	6.74	1.51	0.19
Antarctic Zone													
A3-1	18-Oct-16	50.63°S 72.06°E	2.19	28.21	1.85	19.48	52	1.44	3.66	19.5	2.88	150.70	5.40
A3-2	24-Oct-16	50.63°S 72.06°E	2.06	28.11	1.84	19.85	51	1.64	4.88	17.6	1.59	138.30	4.50
KER	18-Oct-16	50.68°S 68.38°E	2.38	28.23	1.97	18.41	51	0.32	2.89	15.6	5.37	13.52	3.88
FS	19-Oct-16	52.50°S 67.00°E	2.00	29.36	1.96	21.90	52	0.28	2.81	9.4	5.23	10.07	2.15
O11	20-Oct-16	56.50°S 63.00°E	1.00	29.90	2.01	30.95	46	0.27	2.30	3.4	4.00	13.72	1.62
SI	21-Oct-16	58.50°S 61.50˚E	-1.12	29.27	1.87	35.89	48	0.22	1.88	b.d.	2.23	13.36	3.10

∑N = nitrate + nitrite; DOC = dissolved organic carbon; Chl *a* = chlorophyll *a*; BA = bacterial abundance; Synecho = Synechococcus; Pico-Nano = Pico-Nanophytoplankton; Dinoflag = Dinoflagellates; n.a = data not available; b.d. = below detection. Salinity and concentrations of dissolved oxygen are provided in Table S1.

Table 1. Brief description of the study sites. All values are from 10m depth.

Station	Date	Lat/ Long	Temp (°C)	∑N (µM)	PO_4^{3-} (µM)	$Si(OH)_4$ (µM)	DOC (µM)	Chl *a* (µg L^{-1})	BA (x$10^8 L^{-1}$)	Synecho (x$10^4 L^{-1}$)	PicoNano (x $10^6 L^{-1}$)	Diatoms (x $10^4 L^{-1}$)	Dinoflag (x $10^4 L^{-1}$)
Subtropical Zone													
O22	08-Oct-16	29.00°S 58.93°E	20.09	0.04	0.04	1.75	76	0.06	5.51	170.0	1.13	0.24	1.96
O24	10-Oct-16	38.00°S 63.65°E	14.60	2.91	0.21	2.37	62	0.29	7.64	3160.0	12.07	14.75	3.55
Subantarctic Zone													
O25	12-Oct-16	45.00°S 67.77°E	7.61	19.06	1.25	2.03	51	0.42	5.05	902.0	9.65	63.20	1.55
Polar Front Zone													
O12	25-Oct-16	47.00°S 72.22°E	4.60	25.42	1.68	7.72	50	0.39	6.02	134.0	4.79	14.52	3.44
TNS6	15-Oct-16	48.78°S 72.28°E	2.92	26.51	1.93	13.93	52	1.02	3.94	57.4	3.86	64.40	11.40
BDT	17-Oct-16	49.50°S 69.21°E	2.94	26.30	1.81	14.29	68	n.a	4.46	47.7	6.74	1.51	0.19
Antarctic Zone													
A3-1	18-Oct-16	50.63°S 72.06°E	2.19	28.21	1.85	19.48	52	1.44	3.66	19.5	2.88	150.70	5.40
A3-2	24-Oct-16	50.63°S 72.06°E	2.06	28.11	1.84	19.85	51	1.64	4.88	17.6	1.59	138.30	4.50
KER	18-Oct-16	50.68°S 68.38°E	2.38	28.23	1.97	18.41	51	0.32	2.89	15.6	5.37	13.52	3.88
FS	19-Oct-16	52.50°S 67.00°E	2.00	29.36	1.96	21.90	52	0.28	2.81	9.4	5.23	10.07	2.15
O11	20-Oct-16	56.50°S 63.00°E	1.00	29.90	2.01	30.95	46	0.27	2.30	3.4	4.00	13.72	1.62
SI	21-Oct-16	58.50°S 61.50˚E	-1.12	29.27	1.87	35.89	48	0.22	1.88	b.d.	2.23	13.36	3.10

∑N = nitrate + nitrite; DOC = dissolved organic carbon; Chl *a* = chlorophyll *a*; BA = bacterial abundance; Synecho = Synechococcus; Pico-Nano = Pico-Nanophytoplankton; Dinoflag = Dinoflagellates; n.a = data not available; b.d. = below detection. Salinity and concentrations of dissolved oxygen are provided in Table S1.

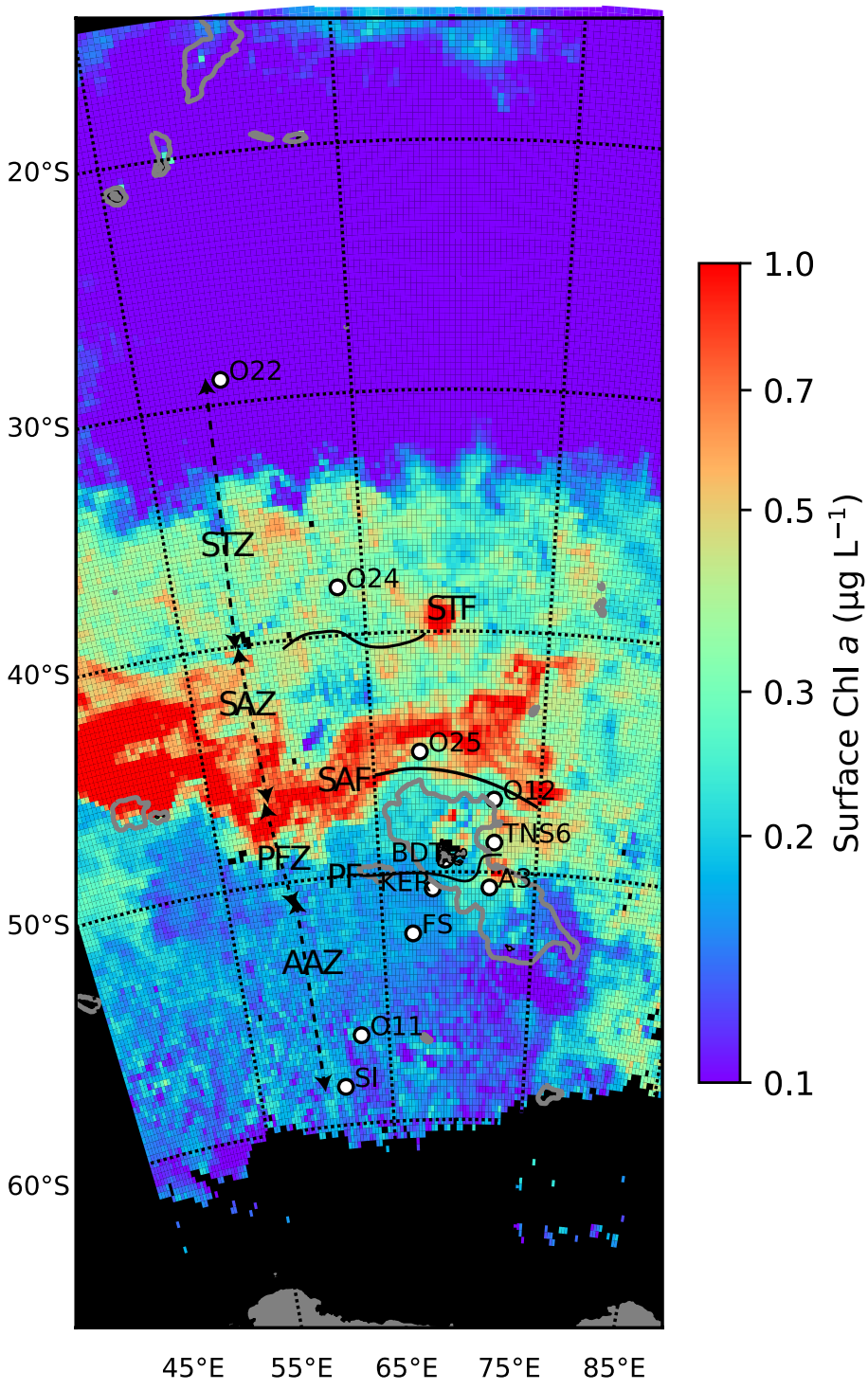
20°S
30°S
40°S
50°S
60°S
45°E
55°E
65°E
75°E
85°E
O22
O24
O25
O12
TNS6
A3
FS
O11
SI
KER
STZ
STF
SAZ
SAF
PFZ
PF
AAZ
1.0
0.7
0.5
0.3
0.2
0.1
Surface Chl a (µg L⁻¹)

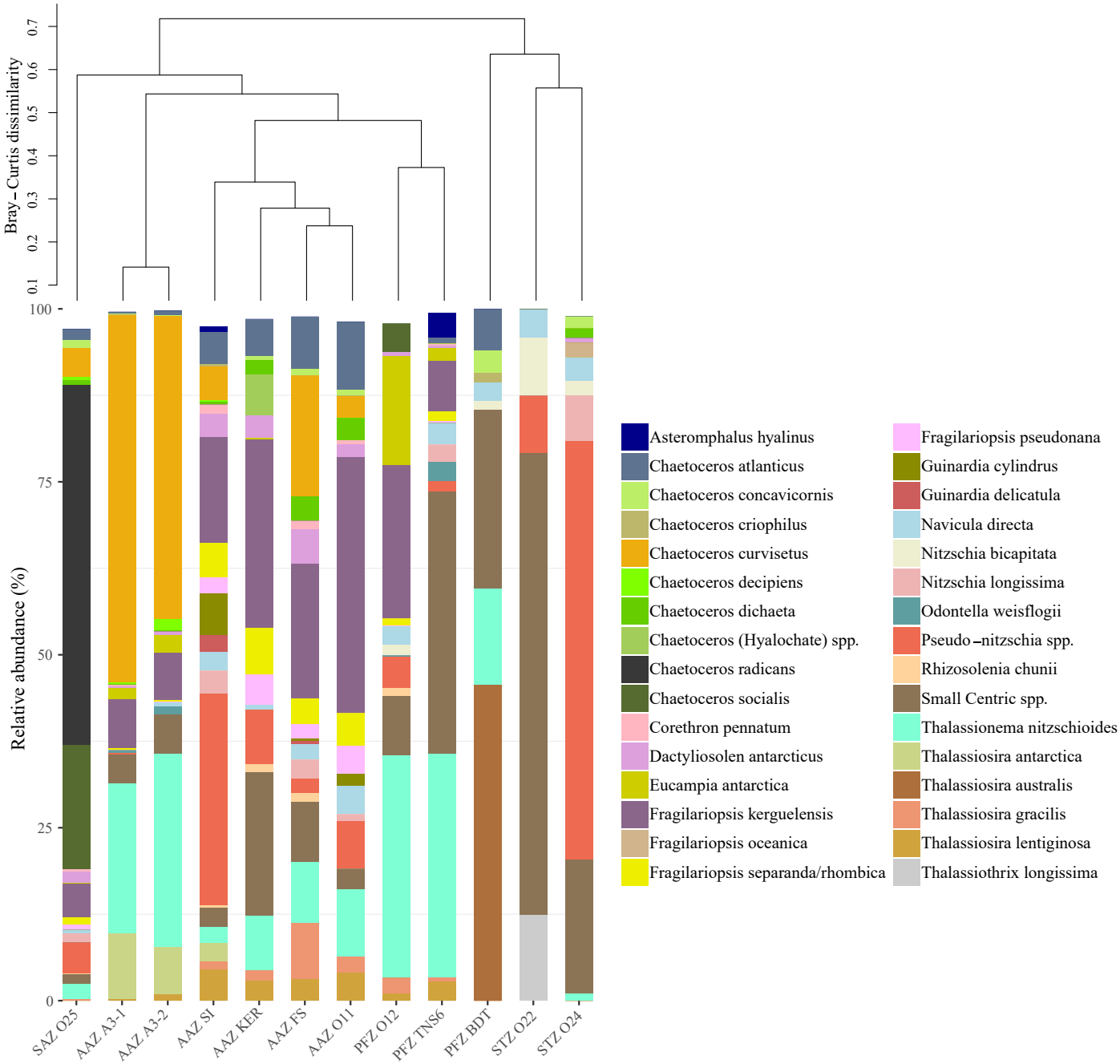
Bray – Curtis dissimilarity
0.1
0.2
0.3
0.4
0.5
0.6
0.7
Relative abundance (%)
100
75
50
25
0
SAZ O25
AAZ A3-1
AAZ A3-2
AAZ SI
AAZ KER
AAZ FS
AAZ O11
PFZ O12
PFZ TNS6
PFZ BDT
STZ O22
STZ O24
Asteromphalus hyalinus
Chaetoceros atlanticus
Chaetoceros concavicornis
Chaetoceros criophilus
Chaetoceros curvisetus
Chaetoceros decipiens
Chaetoceros dichaeta
Chaetoceros (Hyalochate) spp.
Chaetoceros radicans
Chaetoceros socialis
Corethron pennatum
Dactyliosolen antarcticus
Eucampia antarctica
Fragilariopsis kerguelensis
Fragilariopsis oceanica
Fragilariopsis separanda/rhombica
Fragilariopsis pseudonana
Guinardia cylindrus
Guinardia delicatula
Navicula directa
Nitzschia bicapitata
Nitzschia longissima
Odontella weisflogii
Pseudo–nitzschia spp.
Rhizosolenia chunii
Small Centric spp.
Thalassionema nitzschioides
Thalassiosira antarctica
Thalassiosira australis
Thalassiosira gracilis
Thalassiosira lentiginosa
Thalassiothrix longissima

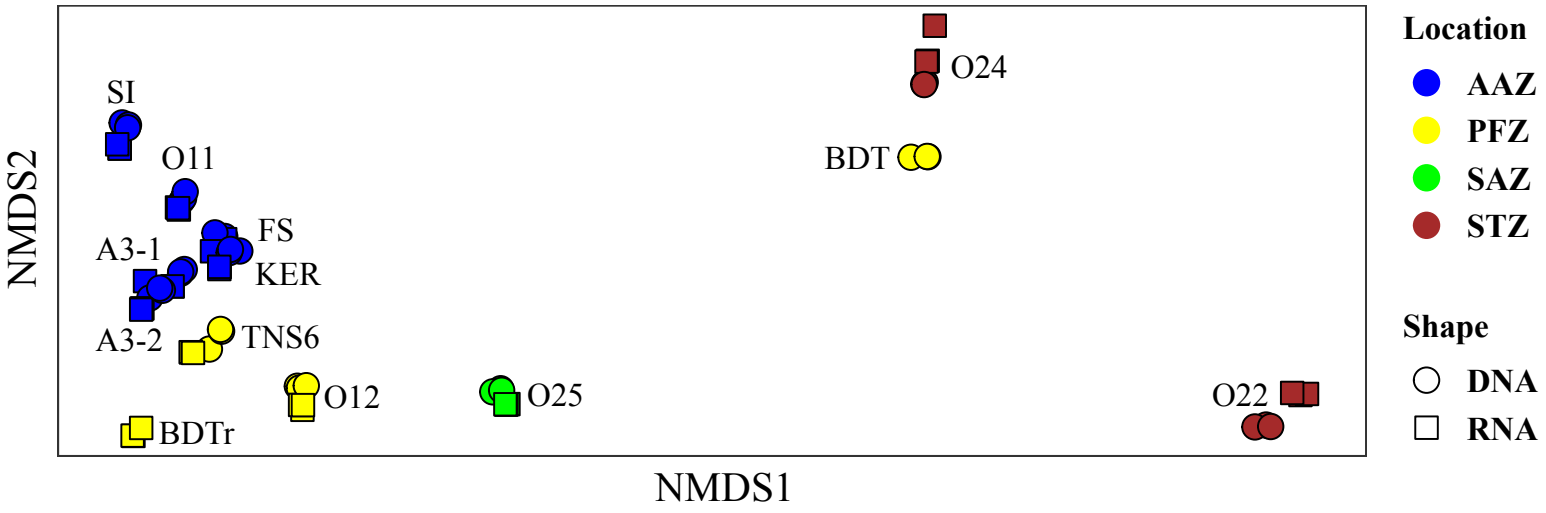
SI
O11
FS
A3-1
KER
A3-2
TNS6
O12
O25
BDTr
O24
BDT
O22
NMDS2
NMDS1
Location
AAZ
PFZ
SAZ
STZ
Shape
DNA
RNA

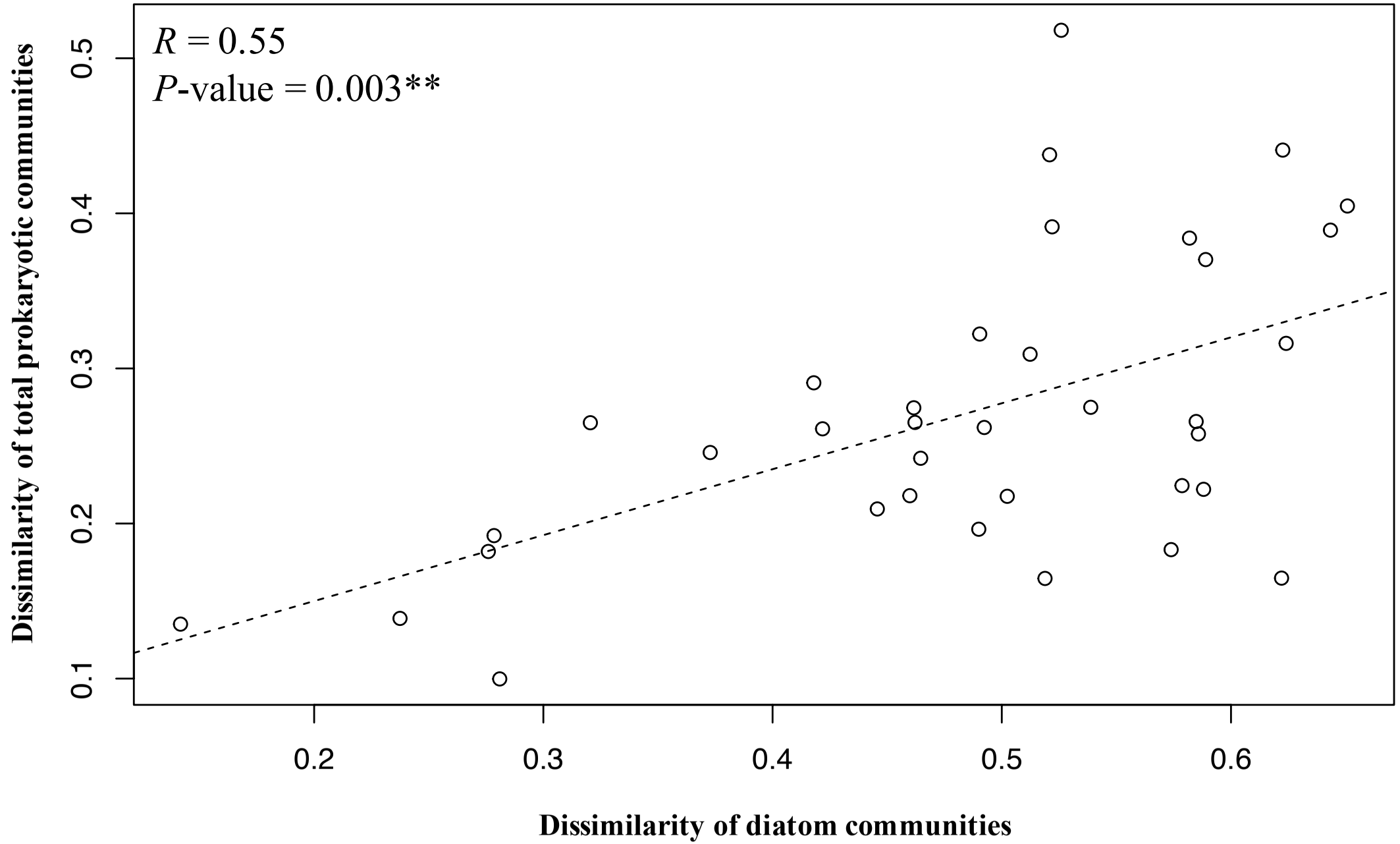
R = 0.55
P-value = 0.003**
Dissimilarity of total prokaryotic communities
0.1
0.2
0.3
0.4
0.5
0.2
0.3
0.4
0.5
0.6
Dissimilarity of diatom communities

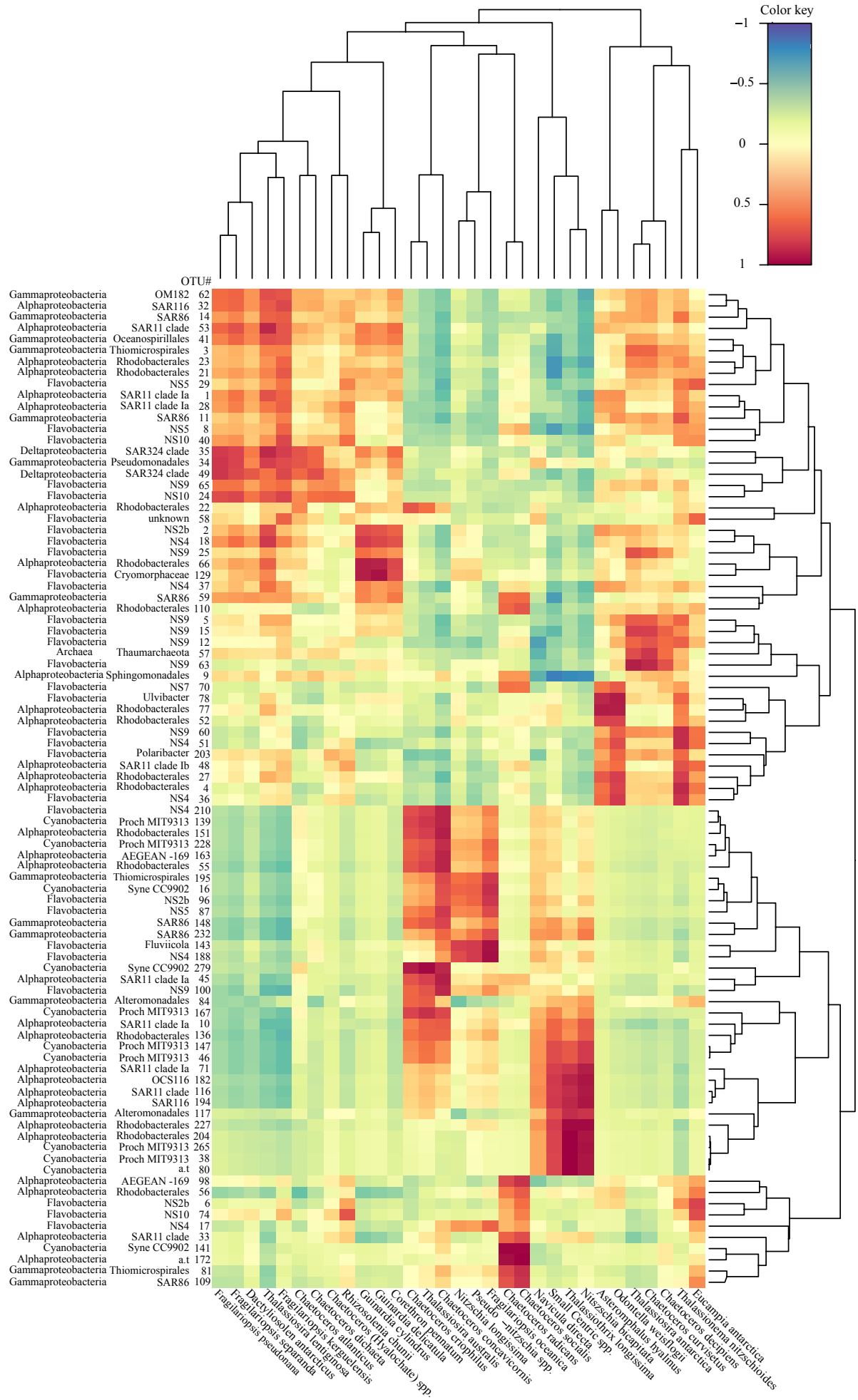
Color key
−1
−0.5
0
0.5
1
OTU#
Gammaproteobacteria OM182 62
Alphaproteobacteria SAR116 32
Gammaproteobacteria SAR86 14
Alphaproteobacteria SAR11 clade 53
Gammaproteobacteria Oceanospirillales 41
Gammaproteobacteria Thiomicrospirales 3
Alphaproteobacteria Rhodobacterales 23
Alphaproteobacteria Rhodobacterales 21
Flavobacteria NS5 29
Alphaproteobacteria SAR11 clade Ia 1
Alphaproteobacteria SAR11 clade Ia 28
Gammaproteobacteria SAR86 11
Flavobacteria NS5 8
Flavobacteria NS10 40
Deltaproteobacteria SAR324 clade 35
Gammaproteobacteria Pseudomonadales 34
Deltaproteobacteria SAR324 clade 49
Flavobacteria NS9 65
Flavobacteria NS10 24
Alphaproteobacteria Rhodobacterales 22
Flavobacteria unknown 58
Flavobacteria NS2b 2
Flavobacteria NS4 18
Flavobacteria NS9 25
Alphaproteobacteria Rhodobacterales 66
Flavobacteria Cryomorphaceae 129
Flavobacteria NS4 37
Gammaproteobacteria SAR86 59
Alphaproteobacteria Rhodobacterales 110
Flavobacteria NS9 5
Flavobacteria NS9 15
Flavobacteria NS9 12
Archaea Thaumarchaeota 57
Flavobacteria NS9 63
Alphaproteobacteria Sphingomonadales 9
Flavobacteria NS7 70
Flavobacteria Ulvibacter 78
Alphaproteobacteria Rhodobacterales 77
Alphaproteobacteria Rhodobacterales 52
Flavobacteria NS9 60
Flavobacteria NS4 51
Flavobacteria Polaribacter 203
Alphaproteobacteria SAR11 clade Ib 48
Alphaproteobacteria Rhodobacterales 27
Alphaproteobacteria Rhodobacterales 4
Flavobacteria NS4 36
Flavobacteria NS4 210
Cyanobacteria Proch MIT9313 139
Alphaproteobacteria Rhodobacterales 151
Cyanobacteria Proch MIT9313 228
Alphaproteobacteria AEGEAN -169 163
Alphaproteobacteria Rhodobacterales 55
Gammaproteobacteria Thiomicrospirales 195
Cyanobacteria Syne CC9902 16
Flavobacteria NS2b 96
Flavobacteria NS5 87
Gammaproteobacteria SAR86 148
Gammaproteobacteria SAR86 232
Flavobacteria Fluviicola 143
Flavobacteria NS4 188
Cyanobacteria Syne CC9902 279
Alphaproteobacteria SAR11 clade Ia 45
Flavobacteria NS9 100
Gammaproteobacteria Alteromonadales 84
Cyanobacteria Proch MIT9313 167
Alphaproteobacteria SAR11 clade Ia 10
Alphaproteobacteria Rhodobacterales 136
Cyanobacteria Proch MIT9313 147
Cyanobacteria Proch MIT9313 46
Alphaproteobacteria SAR11 clade Ia 71
Alphaproteobacteria OCS116 182
Alphaproteobacteria SAR11 clade 116
Alphaproteobacteria SAR116 194
Gammaproteobacteria Alteromonadales 117
Alphaproteobacteria Rhodobacterales 227
Alphaproteobacteria Rhodobacterales 204
Cyanobacteria Proch MIT9313 265
Cyanobacteria Proch MIT9313 38
Cyanobacteria a.t 80
Alphaproteobacteria AEGEAN -169 98
Alphaproteobacteria Rhodobacterales 56
Flavobacteria NS2b 6
Flavobacteria NS10 74
Flavobacteria NS4 17
Alphaproteobacteria SAR11 clade 33
Cyanobacteria Syne CC9902 141
Alphaproteobacteria a.t 172
Gammaproteobacteria Thiomicrospirales 81
Gammaproteobacteria SAR86 109
Fragilariopsis pseudonana
Fragilariopsis separanda
Dactyliosolen antarcticus
Thalassiosira lentiginosa
Fragilariopsis kerguelensis
Chaetoceros atlanticus
Chaetoceros dichaeta
Rhizosolenia (Hyalochaete) spp.
Guinardia cylindrus
Guinardia chuni
Corethron pennatum
Chaetoceros decipiens
Thalassiosira australis
Chaetoceros criophilus
Nitzschia longissima
Pseudo−nitzschia spp.
Fragilariopsis oceanica
Chaetoceros radicans
Navicula directa
Small Centric spp.
Thalassiothrix longissima
Nitzschia bicapitata
Asterompahalus hyalinus
Odontella weissflogii
Thalassiosira antarctica
Chaetoceros curvisetus
Thalassionema nitzschioides
Eucampia antarctica